Stark Effect in Perovskite/TiO$_2$ Solar Cells: Evidence of Local Interfacial Order

Vittoria Roiati,[†,‡,#] Edoardo Mosconi,[§] Andrea Listorti,*[,†,‖] Silvia Colella,[‖] Giuseppe Gigli,[†,‖,⊥] and Filippo De Angelis*[,§]

[†]Center for Bio-Molecular Nanotechnology, Fondazione Istituto Italiano di Tecnologia, Via Barsanti, 73010 Arnesano (Lecce), Italy

[‡]Department of Physics, Politecnico di Milano, p.zza Leonardo da Vinci 32, Milano, Italy

[§]Computational Laboratory for Hybrid/Organic Photovoltaics (CLHYO), CNR-ISTM, Via Elce di Sotto 8, Perugia I-06123, Italy

[‖]NNL − National Nanotechnology Laboratory, CNR Istituto Nanoscienze, Distretto Tecnologico, Via Arnesano 16, 73100 Lecce, Italy

[⊥]Dipartimento di Matematica e Fisica "E. De Giorgi", Universita' del Salento, Via per Arnesano, 73100 Lecce, Italy

[#]Center for Nano Science and Technology@Polimi, Istituto Italiano di Tecnologia, Via G. Pascoli 70/3, 20133 Milano, Italy

S *Supporting Information*

ABSTRACT: To unveil the mechanisms controlling photovoltaic conversion in high-performing perovskite-based meso-structured solar cells, we focus on the key role played by the mesoporous oxide/perovskite interface. We employ several spectroscopic techniques to design a complete scenario and corroborate our results with first principle density functional theory calculations. In particular Stark spectroscopy, a powerful tool allowing interface-sensitive analysis is employed to prove the existence of oriented permanent dipoles, consistent with the hypothesis of an ordered perovskite layer, close to the oxide surface. The existence of a structural order, promoted by specific local interactions, could be one of the decisive reasons for highly efficient carriers transport within perovskite films.

KEYWORDS: *Perovskites, hybrid solar cells, Stark spectroscopy, DFT investigations*
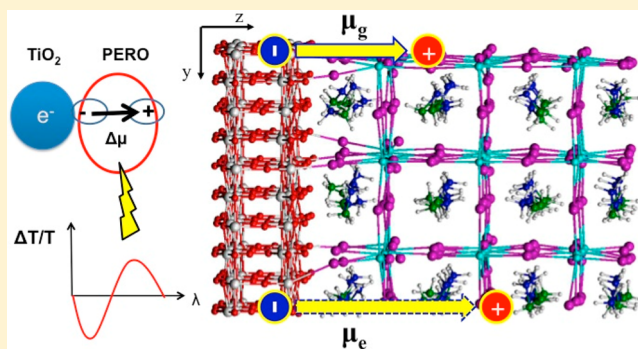
The recent employment of self-assembling lead-halide hybrid perovskites in solar cell devices has been depicted as the "Next Big Thing in Photovoltaics".[1] The observation origins from the numerous advantages related to the introduction of these eclectic materials in solar cells. The employed perovskites strongly absorb light over a broad range, enabling the complete harvesting of a wide portion of solar spectrum in films as thin as few hundred nanometers. This is specifically beneficial when perovskites are included, as sensitizers, in meso-structured (MS) solid-state cells, where the thickness of the mesoporous scaffold has been historically limiting light harvesting and photocurrent generation.[2] In addition, through the perovskite matrix both electrons and holes can percolate to the contacts with a collection efficiency close to unity, giving the opportunity to largely overcome the limitations of previous device layouts.[3] For these characteristics, perovskite solar cells have been assembled in a variety of architectures, either in MS or planar thin film devices, involving different preparation routes and possibly morphology of the final compounds.[4−8]

Despite the rapid increase in efficiency associated with the evolution of this technology, many of the fundamental questions concerning the material properties, deeply related to device operation, remain unanswered. In particular, understanding the interplay of the perovskite morphology and crystalline structure and the role of the MS scaffold in affecting device performances represent a major challenge. This is due to the peculiar self-assembling process, led by weak interactions, through which the perovskite is formed within the oxide pores, so that the material final conformation largely depends on the assembling conditions.[9−11]

To shed light on this very peculiar aspect, PL-quenching measurements, among other spectroscopic investigations, have been recently carried out to determine the exciton diffusion length in perovskite films included in different device configurations. In flat donor/acceptor heterojuction samples, perovskite was coupled with diverse charge extracting materials (e.g., NiO, PEDOT:PSS, V$_2$O$_5$, and Spiro-OMeTAD as hole acceptor media or TiO$_2$ and fullerene derivatives as electron
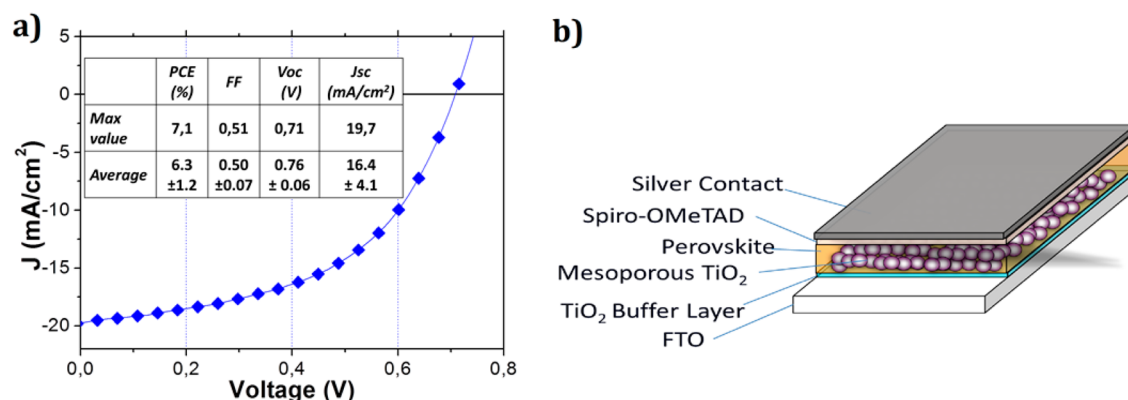
Figure 1. (a) $I-V$ curves under illumination of the best performing device. Inset: table showing the maximum obtained value of the average performances calculated over a series of 14 devices. (b) Sketch of the hybrid device structure. Samples for spectroscopic analysis hold the very same structure with TiO_2 or Al_2O_3 MS scaffold, but an insulator layer is employed instead of Spiro-OMeTAD. The reference for flat perovskite is fabricated on a silica substrate.

acceptor media),[12−14] and the exciton diffusion length was found to extend up to 1 μm for the $CH_3NH_3PbI_{3−x}Cl_x$ mixed halide compound. In these reports, an exciton binding energy of about 50 meV, a value previously determined for $CH_3NH_3PbI_3$ orthorhombic crystalline phase, was retrieved. Intriguingly, in recent works, exciton binding energy was found to be dependent on the perovskite surrounding media and on its assembling conditions. For example, the presence of plasmonic nanoparticles in a perovskite film was found to contribute to the exciton relaxation, leading to increased PL-quenching and improved charge generation.[15] Most interestingly, Choi et al. recently demonstrated that perovskite formation in a mesoporous titanium dioxide also affects the PL-quenching mechanisms,[16] primarily influencing the crystalline order. In particular two diverse perovskite phases were distinguished within the oxide pores: a medium range ordered perovskite crystallite and a short-range structural coherent component in the form of nanoparticles. The photoluminescent behavior was associated to the disordered phase, while the crystalline material was found to be nonemissive. Therefore, in a mesoporous TiO_2 scaffold, an improved material structural coherence could enhance the PL-quenching, in comparison to a flat TiO_2/perovskite configuration. The collection of those results is a strong proof of the key role played by the interface between perovskite film and oxide substrate in influencing the active material properties and hence photovoltaic conversion mechanisms and device performances.

Here, we focus on the mixed-halide $CH_3NH_3PbI_{3−x}Cl_x$ perovskite (hereafter PERO) deposited onto a MS TiO_2 scaffold, with particular emphasis placed on the role played by the TiO_2/PERO interface. As a comparison with traditional dye-sensitized solar cells (DSCs), we also investigate the TiO_2 interface with the prototypical D149 organic dye. Combining several spectroscopic techniques and first-principles computational analyses, we demonstrate the existence of a locally ordered perovskite layer close to the oxide surface, induced by specific interactions occurring between the oxide surface and the self-assembled perovskite.

The above-mentioned phenomena were observed in a series of state-of-the-art devices, whose performances are resumed in Figure 1, realized with identical geometry and procedure as the ones used for the spectroscopical investigations. The existence of local order at the interface between perovskite and oxide could be one of the decisive reasons for the high-performance

characterizing devices based on MS-TiO_2 and in particular could help in rationalizing the highly efficient carrier transport occurring within the perovskite film.[17]

To trace a complete picture of interface-induced processes, we performed time-correlated single photon counting (TCSPC) analysis, photoinduced absorption spectroscopy (cw-PIA), and electroabsorption (EA) measurements on model samples reproducing the core structure of high-performing devices.

To investigate the PL-quenching in our systems, we prepared two MS model samples, holding the same PERO material assembled onto Al_2O_3 and TiO_2 matrix, and a reference PERO film deposited on flat glass, see Figure 1b for sample structures. The TCSPC decays for PERO in the three considered systems are reported in Figure 2a. As expected, the PERO PL is completely quenched (99%) within the TiO_2 pores, as compared with PERO deposited on glass. Interestingly, in Al_2O_3 pores a reasonably strong PL quenching occurs (~20%), even though the charges cannot be extracted given the insulating nature of the scaffold. Consequently, this quenching must be related to an interaction between the perovskite and the oxide surface, which is independent from interfacial electron transfer processes. Two possible effects could take place in these systems in justifying this observation: a specific oxide/perovskite precursor chemical interaction, affecting the material growth, and/or a mere nonspecific physical confinement imposed by the pores, affecting the self-assembling process. Noticeably, both these effects would also be present when the perovskite is assembled into a MS-TiO_2 matrix.

To directly monitor charge extraction in MS-TiO_2/PERO/ PMMA systems we performed continuous wavelength (cw) photo-induced absorption (PIA) measurements. In cw-PIA, an on/off monochromatic continuum laser source provides the excitation flux while the differential transmission of white light probes the photogenerated species. This spectroscopic tool is widely used for the determination of generation and recombination of charge carriers in the microseconds− milliseconds time domain in dye-sensitized solar cells.[5,18,19] In Figure 2b, we compare the near-infrared PIA spectrum of MS-TiO_2/PERO/PMMA with that of MS-TiO_2 sensitized by the D149 dye.[20] D149 is a standard dye for the realization of solid-state DSCs, allowing high-charge generation when adsorbed onto thin TiO_2 photanodes.[20] The two samples considered for this study were fabricated to give comparable characteristics
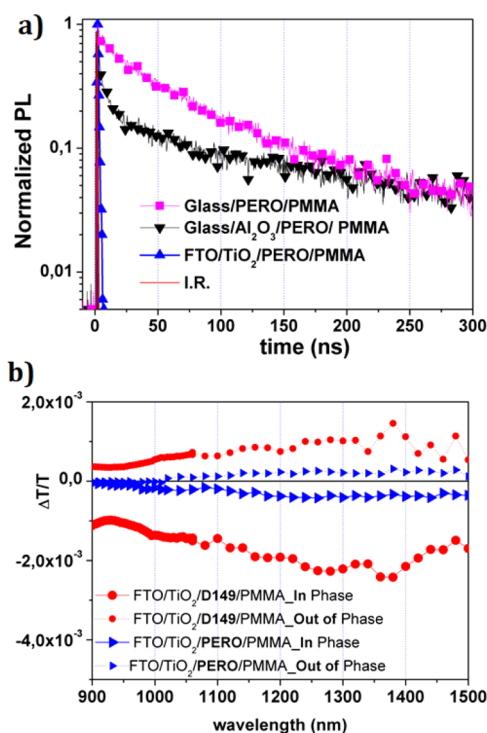
Figure 2. (a) TCSPC decays for PERO in MS-TiO$_2$/PERO/PMMA (red dots), MS-Al$_2$O$_3$/PERO/PMMA (black triangles), and glass/PERO/PMMA (blue squares). (b) In-phase and out-of-phase PIA spectra of MS-TiO$_2$/PERO/PMMA (blue triangles) and MS-TiO2/D149/PMMA (red dots). MS-TiO$_2$/PERO/PMMA spectra have 10× magnification.

in terms of light absorption at the excitation wavelength λ_{exc} = 488 nm (see Supporting Information for sample description and Figure S1 for absorption characteristics). Comparing the two PIA curves of Figure 2b, it immediately appears that the broad negative signal assigned to the absorption of TiO$_2$-

injected electrons in the 900−1500 nm region is almost 2 orders of magnitude smaller in the case of PERO with respect to D149. The intensity of each PIA feature is directly related to the formation yield of photogenerated species and to their recombination dynamics; noticeably, the mentioned signal is symmetrically collected both in the in-phase and out-of-phase PIA spectra of Figure 2b and this is an established fingerprint of long-living species (up to milliseconds).[20,21] This measurement proves that only a fraction of photogenerated electrons are injected into the TiO$_2$ matrix with known long living dynamics, so the observed PL-quenching cannot be straightforwardly associated to charge injection form the perovskite absorber to MS-TiO$_2$. This hypothesis and the existence of a related double path for carriers collection in MS perovskite based devices has been recently demonstrated with a complete spectroscopic investigation.[22] Noticeably, a similar conclusion has been also drawn for CH$_3$NH$_3$PbI$_3$ and CH$_3$NH$_3$PbI$_{3-x}$Cl$_x$ perovskites by means of electrochemical impedance spectroscopy measurements,[17,23] supporting our observations.

In Figure 3, we report the PIA spectrum of MS-TiO$_2$/PERO/PMMA in the visible region of the spectrum collected at 170 Hz pump modulation. Three distinguished regions dominate the spectrum: a negative feature spreading from 600 to 720 nm, a sharp positive feature peaking at 750 nm and a negative signal above 780 nm extending in the whole near-IR spectral region, the latter attributable to absorption of TiO$_2$-injected electrons (see also Figure 2b). The two features below 780 nm cannot be easily associated to known photogenerated species. These features can notably be observed only in the in-phase component of the PIA spectrum, suggesting a faster recovering dynamics compared to the characteristic dynamics of electrons into the MS-TiO$_2$ matrix. The peculiar PIA spectral shape and recombination dynamics, however, seem to resemble what previously observed for organic dyes absorbed on TiO$_2$, when a Stark effect is perturbing the ground-state absorption.[24−28] We therefore hypothesize the presence of a similar
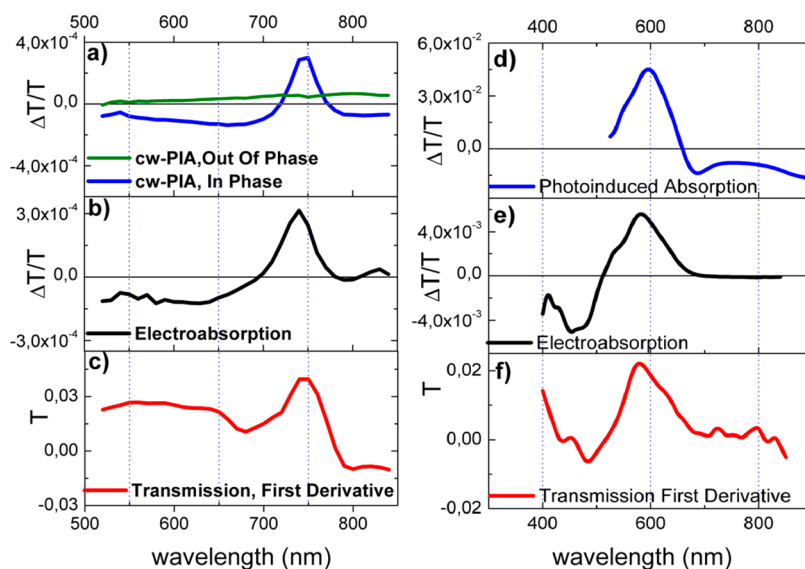

Figure 3. (a) In-phase and out-of-phase photoinduced absorption (PIA) spectra of MS-TiO$_2$/PERO/PMMA. (b) EA of MS-TiO$_2$/PERO/PMMA/Ag sample with negative field polarity applied to the FTO/TiO$_2$ contact. (c) First derivative of MS-TiO$_2$/PERO/PMMA transmission spectrum obtained with the same setup employed for the other measurements. (d) In-phase PIA spectrum of MS-TiO$_2$/D149/PMMA. (e) EA spectrum of MS-TiO$_2$/D149/PMMA/Ag sample with negative field polarity applied to the FTO/TiO$_2$ contact. (f) First derivative of MS-TiO$_2$/D149/PMMA transmission spectrum obtained with the same setup employed for the other measurements.

C

dx.doi.org/10.1021/nl500544c | Nano Lett. XXXX, XXX, XXX−XXX

condition also in the MS-TiO$_2$/perovskite system here investigated.

The origin of Stark shifts in dye-sensitized interfaces was interpreted in terms of local electric fields generated by TiO$_2$-injected electrons and possibly by oxidized dyes on the ground state absorption of neighboring dyes.[24−28]

In the archetypical cases of traditional DSCs based on organic sensitizers, the effect was proven to be linearly dependent on the applied electric field, because dyes absorbed on the TiO$_2$ surface held an oriented permanent dipole. The Stark spectral response was shown to depend on the variation of the dipole moment between the ground (μ_i) and the excited (μ_f) state of the dye with respect to the interfacial electric field direction, that is, to the direction perpendicular to the oxide surface.[29] As in the case of traditional DSCs, we employed electroabsorption spectroscopy (EA) to prove the existence of a Stark effect, possibly reproducing the observed PIA spectral features. In Figure 3b, the EA spectrum of the FTO/MS-TiO$_2$/PERO/PMMA/Ag sample is reported. An oscillating field with superimposed direct current (dc) bias was applied with negative or positive polarity on the FTO contact and grounded Ag contact. Most notably, the EA spectrum clearly reproduces the PIA results, Figure 3a. Figure 3c also shows the first derivative of the transmittance spectrum of the FTO/MS-TiO$_2$/PERO/PMMA sample, whose shape agreeably reproduces both the EA and the PIA features. As a separate test, we investigated the effect of changing the dc component of the modulated voltage on the EA spectra and found that the amplitude of the EA signal increased linearly with the voltage, see Figure 4.
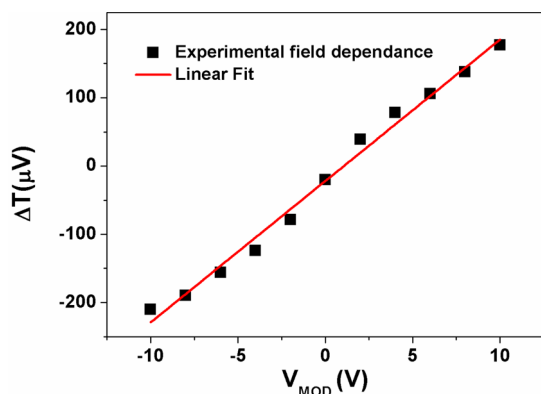

Figure 4. Electroabsorption intensity as a function of bias voltage (dc component, given fixed 20 V alternating current component) recorded at 750 nm for FTO/MS-TiO$_2$/PERO/PMMA/Ag sample. The red line indicates a linear fit to the data.

Markedly this is also a direct proof of the absence of free charges injected from the contacts, as their superposition would provide spectral features not affected by dc voltage variation.[30] Moreover the presence of the insulating PMMA is preventing the massive leakage from silver contact, so we would expect a different contribution by possible absorption of free carriers when the two opposite polarities are applied, see Figure S2, Supporting Information.

Taken together, all the presented evidence prove that the measured effect is linear in the electric field and hence that we are in the presence of a first order Stark effect.

The results above can be rationalized in a coherent framework following linear Stark theory, summarized in eq 1, which describes the absorption variation $\Delta\alpha$, when an electric field F is applied to a system holding a permanent ground state dipole moment μ_g. In the case of a randomly oriented ensemble of molecular dipoles, the first term of the equation vanishes and the Stark effect is proportional to the square of the applied field through the second derivative of the absorption spectrum. In the particular case of coherently oriented dipoles, the first, linear, term dominates over the second term and the spectrum follows a first derivative feature. This is clearly the case of our experimental results, so we can safely conclude that the investigated TiO$_2$/PERO interface exhibits an ensemble of oriented dipole moments.

$$\Delta\alpha = \frac{\partial\alpha}{\partial E}\Delta\mu\cdot F + \frac{1}{2}\frac{\partial^2\alpha}{\partial^2 E}(\Delta\mu\cdot F)^2 \qquad (1)$$

With $\Delta\mu$ given by the difference between the excited state dipole μ_e and ground state dipole μ_g.

Noticeably, the shape of the spectral Stark feature is comparable to the one exhibited by the D149 organic dye in a similar experiment, see Figure 3d−f, therefore we can conclude that the direction of the ground-to-excited state dipole moment variation is the same for both the organic dye and the perovskite sensitizer.[24,26,29]

To further investigate the nature of the interactions occurring at the crucial TiO$_2$/PERO interface, we carried out first principles DFT simulations of a pseudocubic CH$_3$NH$_3$PbI$_3$ perovskite/TiO$_2$ anatase interface. While various first principles calculations have been reported on the electronic and spectroscopic properties of CH$_3$NH$_3$PbI$_3$, see, for example, refs 31−35, this is to our knowledge the first simulation of a organohalide lead perovskite/TiO$_2$ interface. We chose to simulate CH$_3$NH$_3$PbI$_3$ rather than the experimentally employed CH$_3$NH$_3$PbI$_{3-x}$Cl$_x$ perovskite because of the uncertain composition of the latter.[36] Furthermore, the two materials were found to be very similar from a structural point of view, both showing a tetragonal structure at room temperature with very similar cell parameters, within <1%, suggesting a comparably low Cl-incorporation into the MaPbI$_3$ matrix.[11] Our model system is made by a 3 × 5 × 3 pseudocubic perovskite slab exposing one of the equivalent (100), (010), or (001) surfaces, see Figure 5 and Figure S3 in Supporting Information. The perovskite slab stoichiometry is (CH$_3$NH$_3$)$_{60}$Pb$_{45}$I$_{150}$, and thus it deviates from the ideal material stoichiometry, in line with the analysis of perovskites surfaces by Mitzi.[37] To avoid the creation of a permanent dipole within the perovskite slab, the organic cations were initially disposed in a symmetric fashion with respect to the central Pb−I plane. Upon optimization, this structure provided a dipole of only 2.3 D, which reduced to 0.7 D at the TiO$_2$ binding geometry. The considered optimized slab has a calculated band gap of 2.37 eV by scalar relativistic DFT, which reduces to 1.50 eV upon inclusion of spin−orbit coupling.[31,32] These values are higher than those found for the bulk tetragonal phase of the CH$_3$NH$_3$PbI$_3$ perovskite at the same level of theory (1.66/0.60 eV),[31] as expected when moving from a periodic to a confined system. Doubling the perovskite slab along the nonperiodic direction, already provides a converged band gap value compared to the bulk, although this slab is presently too large for computational modeling of the interface.

The perovskite model was "deposited" onto a 5 × 3 × 2 slab of anatase TiO$_2$ made by 120 TiO$_2$ units, exposing the majority (101) surface, see Figure 5 and Figure S3 in Supporting Information. The experimental TiO$_2$ cell parameters (a = 18.92
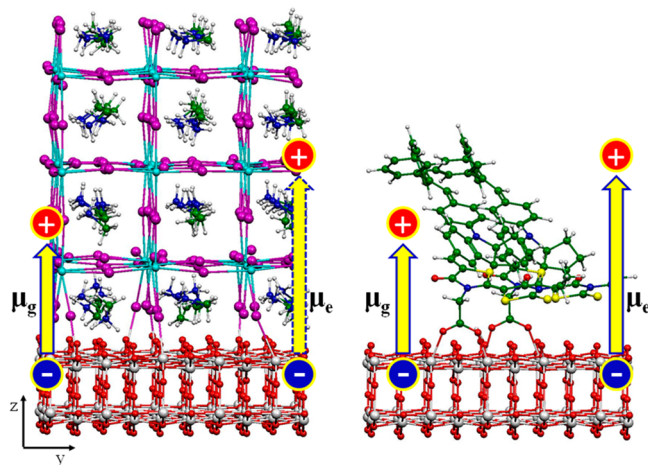
Figure 5. Schematics of calculated ground and excited state dipole moments for the TiO$_2$/PERO and TiO$_2$/D149 interfaces. For the TiO$_2$/PERO system, the excited state dipole moment (dashed) was not calculated but its direction and magnitude can be inferred by similarity with the TiO$_2$/D149 case. The TiO$_2$/D149 interface corresponds to the maximum surface coverage.[39]

Å, b = 30.72 Å) are employed to build a periodic supercell in the x and y directions, leaving 10 Å vacuum along the z direction. The chosen setup introduces a lattice mismatch of only +0.75 and −1.85% along the x and y directions, respectively, compared to the experimental lattice parameter of the pseudocubic perovskite (6.26 Å).[38] Given the slab surface stoichiometry, the TiO$_2$/perovskite interaction occurs mainly through the binding of perovskite iodine atoms to under-coordinated Ti(IV) atoms of the TiO$_2$ surface. Along with the formation of I−Ti chemical bonds, several hydrogen bonds from the methylammonium organic cations to surface oxygen atoms contribute to stabilize the interface. Noticeably, ca. 80% of the surface I atoms are engaged in I−Ti bonds, indicative of the reasonable structural match between the two materials.

The calculated density of states (DOS) for the TiO$_2$/perovskite interface is reported in Figure 6, where the total DOS is decomposed over contributions from the perovskite and the TiO$_2$ fragments. Including spin−orbit coupling, the perovskite conduction band lies quite above the TiO$_2$ conduction band energy, in line with previous DFT results for the noninteracting fragments and with available experimental data.[40,41] Notice, however, that the employed DFT method is prone to underestimate the position of the TiO$_2$ conduction band energy and band gap, so the calculated TiO$_2$/perovskite CB offset (ca. 0.8 eV) is expectedly overestimated. This overestimate is also due to the larger-than-bulk band gap value calculated for the perovskite slab, which likely raises the perovskite CB edge.

As it can be noticed, the two materials are only weakly interacting, as seen by the little hybridization found between the perovskite Pb s-p states, maximally contributing the material conduction band,[31,42] and the Ti d orbitals constituting the TiO$_2$ conduction band. The hybridization can be visualized by comparing the bottom of the conduction band region for the interacting TiO$_2$/MAPbI$_3$ system and for the isolated MAPbI$_3$ cut from the optimized interface, inset of Figure 6. This suggests a weak interfacial electronic coupling, which is in line with the moderate charge-transfer to TiO$_2$ observed here at the MS-TiO$_2$/PERO interface, see Figure 2b. This picture differs significantly with what observed for typical dye-sensitizers for which a strong admixture of dye unoccupied levels with TiO$_2$ conduction band states was repeatedly found.[43,44]

Our calculations also indicate a surface dipole of 28 D for the considered supercell, that is, ∼4.8 D per nm^2 of TiO$_2$ surface, pointing away from the TiO$_2$ surface (i.e., with the negative pole close to the TiO$_2$ surface and the positive pole toward the perovskite), see Figure 5. Notice that this dipole was not present in the perovskite and TiO$_2$ fragments, which have almost vanishing dipole moments at their interacting geometry (0.7 and 0.0 D, respectively). Thus the calculated interfacial dipole moment is originated by the TiO$_2$/perovskite inter-

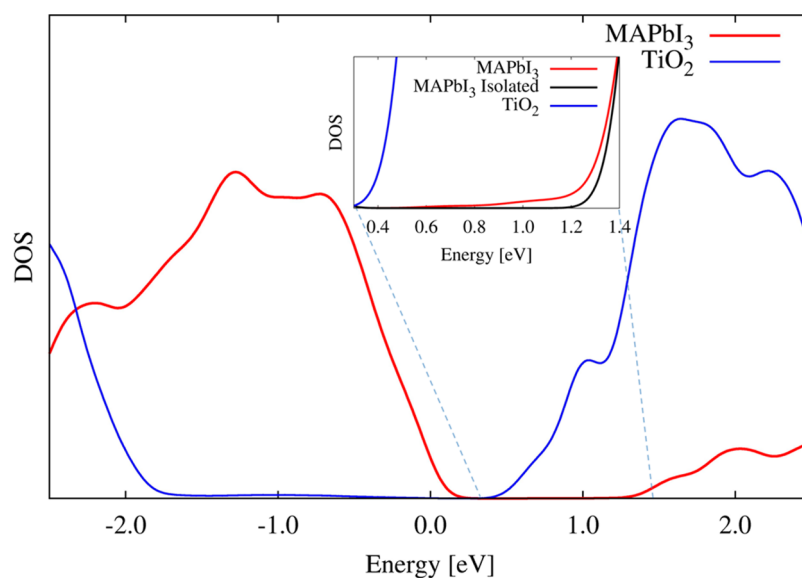**Figure 6.** Calculated DOS including spin−orbit coupling for the TiO$_2$/CH$_3$NH$_3$PbI$_3$ perovskite (MAPbI$_3$) interface, decomposed into the contributions of MAPbI$_3$ (red) and TiO$_2$ (blue). The inset shows the bottom of the interacting perovskite DOS, where hybridization with TiO$_2$ states occurs, compared to the noninteracting perovskite DOS at the same geometry.

action, and it has the same direction as that of typical organic dye sensitizers, see Figure 5 for the comparison with D149.[45]

Considering the similarity of EA/PIA features of PERO and of D149 organic dye, Figure 3, and the ground-state dipole moment direction calculated for TiO_2/perovskite and TiO_2/dye interface, our joint experimental and theoretical data demonstrate the same sign for the dipole moment variation in the two systems. In typical push−pull organic dyes, a dipole moment increase ($\Delta\mu > 0$) is associated to the ground to excited state transition, which results from negative charge accumulation toward the carboxylic TiO_2 anchoring group with the concomitant hole mainly localized toward the outward-pointing donor group, see Figure 5. By analogy, our data suggest a qualitatively similar charge displacement occurring in the MS-TiO_2/PERO interface upon light absorption with negative charge being accumulated (depleted) toward TiO_2 (PERO). We must also notice that a similar Stark effect could be observed even in the absence of charge injected into TiO_2, imputable to the simple migration of holes (electrons) toward the bulk (surface) of the perovskite. However, Stark features are superimposed to PIA signals, see Figure 3, indicating that charges transferred to the mesoporous substrate yet generate a local electric field that reproduces the energetic landscape felt by the system in an EA experiment, despite electron injection to TiO_2 seems not to be a dominating event in MS-TiO_2/PERO systems.

The most interesting conclusion that can be drawn from combined experimental and computational investigation is the presence of oriented permanent dipoles at the MS-TiO_2/PERO interface, prefiguring a locally ordered interfacial region. Experimental and theoretical evidence highlight the key role played by the mesoporous oxide in inducing providing the observed ordered interface. As a further proof, we investigated the isolated perovskite on a flat silica substrate in a similar EA experiment, Figure 7, obtaining evidence of a crucially different response.
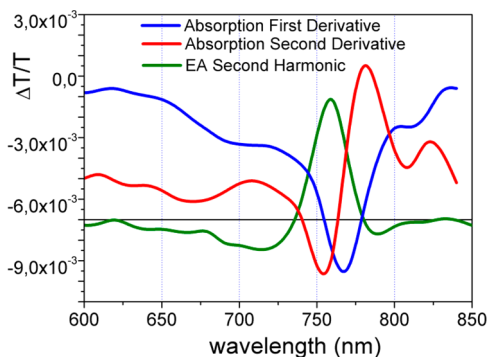

Figure 7. Second harmonic electroabsorption spectrum of PERO film on silica substrate covered by 350 nm of insulating PMMA between FTO and Ag contacts. Spectrum is superimposed to the first and second derivative of the sample absorption spectrum.

EA measurements point out in this case a nonlinear behavior and a mix of first and second derivative signals, revealing the presence of either nonoriented permanent dipoles and/or likely expectable bulk polarization effects, contributing to the Stark signal. These observations clearly differ from the signal recorded on the mesoporous TiO_2 scaffold, though we cannot rule out some (minor) spectral contribution from the material induced polarization. Nevertheless, our observation of a clear

linear trend dominated by first derivative features (Figure 4) shows a dominant contribution due to oriented permanent dipoles, which can therefore straightforwardly be related to the perovskite/TiO_2 interface. Further studies need to be addressed on this topic to decouple the overlapping effects, but two main results emerge from the comparison: first, our technique appears to be interface-sensitive because selective interaction with the substrate can be monitored; second, it gives insight to what observed in TCSPC experiments, as the MS oxide substrates inducing local order in perovskite film, is compatible with the proved PL-quenching mechanisms.[16]

The presence of ground-state-oriented dipoles for the self-assembled perovskite on MS-TiO_2 could determine the conditions for an ordered material growth within the pores, induced by interfacial interactions, allowing midrange crystalline coherence. The reported result could be of paramount importance in understanding the remarkable performances of perovskite-based solar cells, as this ordered layer could be responsible for both the enhancement of free carries generation, proved throughout PL-quenching analysis and the efficient carries percolation to the contact, acting as a good transportation layer. These observations are in line and contribute to explain various very recent results, providing the interpretative basis for further optimization of perovskite-based solar cells.

■ ASSOCIATED CONTENT

Ⓢ Supporting Information

Materials preparation procedure, experimental setup description, devices absorption, EA spectrum for Flat TiO_2/PERO, computational details, and addition computation results. This material is available free of charge via the Internet at http://pubs.acs.org.

■ AUTHOR INFORMATION

Corresponding Authors
*E-mail: andrea.listorti@iit.it (A.L.).
*E-mail: filippo@thch.unipg.it (F.D.A.).
Notes
The authors declare no competing financial interest.

■ ACKNOWLEDGMENTS

■ REFERENCES

(1) Bisquert, J.; Editor, S. *J. Phys. Chem. Lett.* **2013**, 2597−2598.
(2) Yum, J.-H.; Chen, P.; Grätzel, M.; Nazeeruddin, M. K. *ChemSusChem* **2008**, *1*, 699−707.
(3) Snaith, H. J. *J. Phys. Chem. Lett.* **2013**, *4*, 3623−3630.
(4) Liu, M.; Johnston, M. B.; Snaith, H. J. *Nature* **2013**, *501*, 395−8.
(5) Lee, M. M.; Teuscher, J.; Miyasaka, T.; Murakami, T. N.; Snaith, H. J. *Science* **2012**, *338*, 643−647.
(6) Burschka, J.; Pellet, N.; Moon, S.-J.; Humphry-Baker, R.; Gao, P.; Nazeeruddin, M. K.; Grätzel, M. *Nature* **2013**, 3−7.
(7) Laban, W. A.; Etgar, L. *Energy Environ. Sci.* **2013**, *6*, 3249.
(8) Chung, I.; Lee, B.; He, J.; Chang, R. P. H.; Kanatzidis, M. G. *Nature* **2012**, *485*, 486−9.

(9) Eperon, G. E.; Burlakov, V. M.; Docampo, P.; Goriely, A.; Snaith, H. J. *Adv. Funct. Mater.* **2013**, *24*, 151−157.

(10) Baikie, T.; Fang, Y.; Kadro, J. M.; Schreyer, M. K.; Wei, F.; Mhaisalkar, S. G.; Gratzel, M.; White, T. *J. Mater. Chem. A* **2013**, *1*, 5628−5641.

(11) Colella, S.; Mosconi, E.; Fedeli, P.; Listorti, A.; Gazza, F.; Orlandi, F.; Ferro, P.; Besagni, T.; Rizzo, A.; Calestani, G.; Gigli, G.; Angelis, F. De; Mosca, R. *Chem. Mater.* **2013**, *25*, 4613−4618.

(12) Stranks, S. D.; Eperon, G. E.; Grancini, G.; Menelaou, C.; Alcocer, M. J. P.; Leijtens, T.; Herz, L. M.; Petrozza, a.; Snaith, H. J. *Science* **2013**, *342*, 341−344.

(13) Xing, G.; Mathews, N.; Sun, S.; Lim, S. S.; Lam, Y. M.; Gratzel, M.; Mhaisalkar, S.; Sum, T. C. *Science (80-.)* **2013**, *342*, 344−347.

(14) Docampo, P.; Ball, J. M.; Darwich, M.; Eperon, G. E.; Snaith, H. J. *Nat. Commun.* **2013**, *4*, 2761.

(15) Zhang, W.; Saliba, M.; Stranks, S. D.; Sun, Y.; Shi, X.; Wiesner, U.; Snaith, H. J. *Nano Lett.* **2013**, *13*, 4505−4510.

(16) Choi, J. J.; Yang, X.; Norman, Z. M.; Billinge, S. J. L.; Owen, J. S. *Nano Lett.* **2014**, *14*, 127−133.

(17) Gonzalez-Pedro, V.; Juárez-Pérez, E. J.; Arsyad, W. S.; Barea, M.; Fabregat-Santiago, F.; Mora-Sero, I.; Bisquert, J. *Nano Lett.* **2014**, *14*, 888−893.

(18) Boschloo, G.; Hagfeldt, A. *Chem. Phys. Lett.* **2003**, *370*, 381−386.

(19) Cappel, U. B.; Gibson, E. a.; Hagfeldt, A.; Boschloo, G. *J. Phys. Chem. C* **2009**, *113*, 6275−6281.

(20) Snaith, H. J.; Petrozza, A.; Ito, S.; Miura, H.; Grätzel, M. *Adv. Funct. Mater.* **2009**, *19*, 1810−1818.

(21) Anderson, A. Y.; Barnes, P. R. F.; Durrant, J. R.; Regan, B. *J. Phys. Chem. C* **2010**, *114*, 1953−1958.

(22) Roiati, V.; Colella, S.; Lerario, G.; Marco, L. De; Rizzo, A.; Listorti, A.; Gigli, G. *Energy Environ. Sci.* **2014**, DOI: 10.1039/C3EE43991G.

(23) Kim, H.-S.; Mora-Sero, I.; Gonzalez-Pedro, V.; Fabregat-Santiago, F.; Juarez-Perez, E. J.; Park, N.-G.; Bisquert, J. *Nat. Commun.* **2013**, *4*, 2242−2249.

(24) Cappel, U. B.; Feldt, S. M.; Schöneboom, J.; Hagfeldt, A.; Boschloo, G. *J. Am. Chem. Soc.* **2010**, *132*, 9096−101.

(25) Cappel, U. B.; Plogmaker, S.; Johansson, E. M. J.; Hagfeldt, A.; Boschloo, G.; Rensmo, H. *Phys. Chem. Chem. Phys.* **2011**, *13*, 14767−74.

(26) Cappel, U. B.; Smeigh, A. L.; Plogmaker, S.; Johansson, E. M. J.; Hammarstr, L.; Hagfeldt, A.; Boschloo, G. *J. Phys. Chem. C* **2011**, *115*, 4345−4358.

(27) Ardo, S.; Sun, Y.; Staniszewski, A.; Castellano, F. N.; Meyer, G. J. *J. Am. Chem. Soc.* **2010**, *132*, 6696−6709.

(28) Pastore, M.; Angelis, F. De *J. Phys. Chem. Lett.* **2011**, 1261−1267.

(29) Cappel, U. B.; Plogmaker, S.; Johansson, E. M. J.; Hagfeldt, A.; Boschloo, G.; Rensmo, H. *Phys. Chem. Chem. Phys.* **2011**, *13*, 14767−74.

(30) Lane, P. a.; deMello, J. C.; Fletcher, R. B.; Bernius, M. *Appl. Phys. Lett.* **2003**, *83*, 3611−3613.

(31) Mosconi, E.; Amat, A.; Nazeeruddin, K.; Gratzel, M.; De Angelis, F. *J. Phys. Chem. C* **2013**, *117*, 13902−13913.

(32) Even, J.; Pedesseau, L.; Jancu, J.-M.; Katan, C. *J. Phys. Chem. Lett.* **2013**, *4*, 2999−3005.

(33) Brivio, F.; Walker, A. B.; Walsh, A. *APL Mater.* **2013**, *1*, 042111.

(34) Quarti, C.; Grancini, G.; Mosconi, E.; Bruno, P.; Ball, J. M.; Lee, M. M.; Snaith, H. J.; Petrozza, A.; De Angelis, F. *J. Phys. Chem. Lett.* **2014**, 279−284.

(35) Giorgi, G.; Fujisawa, J.; Segawa, H.; Yamashita, K. *J. Phys. Chem. Lett.* **2013**, *4*, 4213−4216.

(36) Ball, J. M.; Lee, M. M.; Hey, A.; Snaith, H. J. *Energy Environ. Sci.* **2013**, 1739−1743.

(37) Mitzi, D. B. *Inorg. Chem.* **2000**, *39*, 6107−13.

(38) Poglitsch, a.; Weber, D. *J. Chem. Phys.* **1987**, *87*, 6373−6378.

(39) Pastore, M.; De Angelis, F. *ACS Nano* **2010**, *4*, 556−562.

(40) Kim, H.-S.; Lee, C.-R.; Im, J.-H.; Lee, K.-B.; Moehl, T.; Marchioro, A.; Moon, S.-J.; Humphry-Baker, R.; Yum, J.-H.; Moser, J. E.; Grätzel, M.; Park, N.-G. *Sci. Rep.* **2012**, *2*, 1−7.

(41) Lindblad, R.; Bi, D.; Park, B.; Oscarsson, J.; Gorgoi, M.; Siegbahn, H.; Odelius, M.; Johansson, E. M. J. *J. Phys. Chem. Lett.* **2014**, 648−653.

(42) Umebayashi, T.; Asai, K.; Kondo, T.; Nakao, a. *Phys. Rev. B* **2003**, *67*, 155405.

(43) De Angelis, F.; Fantacci, S.; Selloni, A.; Nazeeruddin, M. K.; Grätzel, M. *J. Am. Chem. Soc.* **2007**, *129*, 14156−7.

(44) Pastore, M.; Fantacci, S.; De Angelis, F. *J. Phys. Chem. C* **2013**, 3685−3700.

(45) Ronca, E.; Pastore, M.; Belpassi, L.; Tarantelli, F.; De Angelis, F. *Energy Environ. Sci.* **2013**, *6*, 183.